

Experimental Results Analysis for UiTM BWB Baseline-I and Baseline-II UAV Running at 0.1 Mach number

Wirachman Wisnoe, Wahyu Kuntjoro, Firdaus Mohamad, Rizal Effendy Mohd Nasir, Nor F Reduan, Zurriati Ali

Faculty of Mechanical Engineering
Universiti Teknologi MARA (UiTM)
40450 Shah Alam
MALAYSIA

wira_wisnoe@yahoo.com <http://www.uitm.edu.my>

Abstract—This paper presents results analysis for two models of UiTM Blended Wing Body (BWB) UAV tested in UiTM Low Speed Wind Tunnel. The first model is known as the BWB Baseline-I and the new model known as BWB Baseline-II. The Baseline-II has a simpler planform, broader-chord wing and slimmer body compared to its predecessor while maintaining wingspan. The wind-tunnel experiments were executed at around 0.1 Mach number or about 35m/s with 1/6 scaled down model. Baseline-I is designed with centre elevator while Baseline-II uses canard for pitching motion purpose. The experiments were carried out at various elevator and canard deflection angles. The lift coefficient, drag coefficient, pitching moment coefficient, L/D ratio and drag polar curves were plotted to show the performance of aircraft at various angle of attack. For zero elevator and canard deflection the results show similar trends in terms of lift curve, drag curve and pitching moment curves for both aircrafts.

Keywords— Aerodynamics, Blended Wing Body, Unmanned Aerial Vehicle, Wind Tunnel

I. INTRODUCTION

BLENDED Wing Body (BWB) is a concept where fuselage is merged with wing and tail to become a single entity [1]. BWB is a hybrid of flying-wing aircraft and the conventional aircraft where the body is designed to have a shape of an airfoil and carefully streamlined with the wing to have a desired planform[2].

The major advantage of this BWB concept is the way how it generates lift. Conventional aircraft obtains lift from its wings. However, BWB aircraft obtains lift from wings together with fuselage. Besides that, the streamlined shape between fuselage and wing intersection reduces interference drag [3]. The slow evolution of fuselage to wing thickness, when carefully designed, may suggest that more volume

can be stored inside the BWB aircraft, hence, increasing payload and fuel capacity [4]. The BWB concept also combines the advantages of a flying wing with the loading capabilities of a conventional airliner by creating a wide body in the center of the wing to allow space for passengers and cargo.

Universiti Teknologi MARA (UiTM) through the Flight Technology & Testing Centre (FTTC) conducts research and development of Blended Wing Body (BWB) concept. Research on BWB in UiTM is conducted through the development of Unmanned Aerial Vehicle (UAV). As described in the literature, depending on its size UAV can be categorized as large, mini, or micro [5,6]. The preliminary study of BWB Baseline-I is discussed in [7] together with its Computational Fluid Dynamics (CFD) analysis at 0.3 Mach number. The BWB Baseline-I UAV can be seen in Figure 1. The preliminary structural analysis of the BWB Baseline-I has been conducted using finite element model as explained in [8]. The aerodynamic study of the Baseline-I has also been done using wind tunnel at 0.1 Mach number for the basic configuration without elevator deflection [9][10]. The study of the effect of centre elevator deflection was carried out for different elevator angles and explained in [11]. The study was performed using Computational Fluid Dynamics (CFD) at Mach 0.3 for various elevator deflections (+5, +10, -5, -10). Experimental testing in UiTM Low Speed Wind Tunnel at 0.1 Mach number completed the study of the effect of elevator on the aerodynamics performance of Baseline-I. With lessons learned in aerodynamics of Baseline-I design, since 2009, the group started a new design of BWB named Baseline-II. This new aircraft is equipped with a pair of canards in front of its main wings (Figure 2).

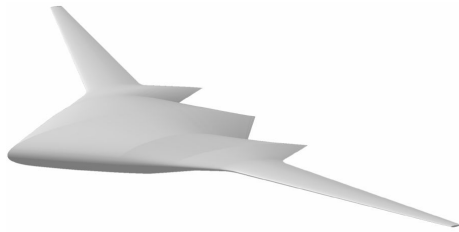


Fig.1: BWB Baseline-I



Fig. 2: BWB Baseline-II

This paper will focus on aerodynamics study for both models of UiTM BWB UAV, i.e. Baseline-I and Baseline-II. Baseline-I is a four-meter span mini UAV class of aircraft with MTOW of 200 kg that shall loiter at its design air speed of Mach 0.1. Baseline-I is designed with an elevator for pitching motion purpose. The Baseline-II actually is a completely-revised, redesigned version of Baseline-I BWB. It has a simpler planform, broader-chord wing and slimmer body than its predecessor while maintaining wing span. The intention is to improve flight performance at low cruising speed by increasing lift-to-drag ratio through planform and shape redesign and inverse twist method on airfoils throughout its span [12]. Follow-up study has been carried out using wind tunnel in order to obtain the aerodynamics characteristic such as lift coefficient, drag coefficient, pitching moment coefficient and L/D ratio. These are discussed in [13-15]

II. MODEL AND WIND TUNNEL SETUP

The experiments were performed in the UiTM low speed wind tunnel (Fig.3). It is a suction type tunnel with a test section area of 0.5 m x 0.5 m x 1.25 m and equipped with 6-Component External Balance. For this study, only 3 components are used with half model of aircraft as the working model.



Fig. 3: UiTM Low Speed Wind Tunnel

Both models are scaled down to 1/6 of the real size. Figure 4 and 5 shows the dimension and manufactured model for Baseline-I and Baseline-II respectively. The experimental parameters for both models are shown in Table 1.

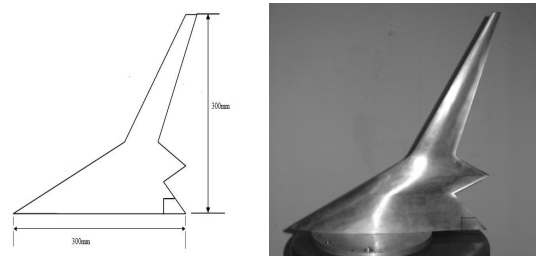


Fig 4: Dimensions and manufactured model of BWB Baseline-I UAV with elevator

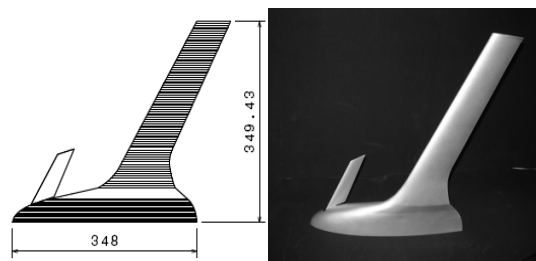


Fig 5: Dimensions and manufactured model of BWB Baseline-II UAV with canard

Table 1: Experimental Parameters

Model	L_{ref}	S_{ref}
Baseline-I	0.336 m	0.04652 m ²
Baseline-II	0.348 m	0.03995 m ²

The experiments were conducted at airspeed of 35 m/s or about 0.1 Mach number at Reynolds number of 8.0×10^5 . The pitching angle (angle of attack) was varied from -10° to $+52^\circ$. Firstly, the elevator and canard deflection were set at zero degree. Then, these control surfaces were set at various deflection angles to obtain aerodynamics data for both aircraft model. Elevator and canard are working as control

surfaces for both aircraft in longitudinal motion mode. Details of the longitudinal mode are discussed in [16, 17].

III. RESULTS AND DISCUSSION

In this section, results from the wind tunnel tests for both models (Baseline-I & Baseline-II) will be presented. The data obtained are plotted to form the lift coefficient versus angle of attack curve, drag coefficient versus angle of attack curve, pitching moment coefficient versus angle of attack curve, drag polar and lift-to-drag versus angle of attack curves.

A. Lift Coefficient

The lift coefficients (C_L) versus angle of attack (α) for both models are shown in Fig.6. From the curve, it is observed that both models show the same trend. The value of C_L increases as angle of attack increases until it reaches its maximum value at around $\alpha = 35^\circ$ for Baseline-I and $\alpha = 42^\circ$ for Baseline-II. The maximum value of C_L produced by Baseline-I is 0.68. The maximum value for Baseline-II is 1.1 which is 61.8% greater than Baseline-I. Small deviations appear at both curves at α around 8° to 10° . The small deviation for Baseline-I curve is due to the flow separation, which occurs on the wing part as shown in Figure 7. Figure 7 shows visualization using mini tuft. It can be seen that the flow is still attached to the overall surface at $\alpha = 7^\circ$. However, at $\alpha = 8^\circ$, the flow has almost completely separated from the wing, except around the wing tip. It means that, beyond this angle of attack, only the body produces the lift for the whole aircraft. For Baseline-II, the small deviation of the curve may also come from the flow separation on the wing part and/or maybe due to the existing of canard in front of the wings. Further investigation is required to clarify the phenomenon that causes the reduction of lift around this pitching angle. Table 2 summarizes some quantitative values obtained.

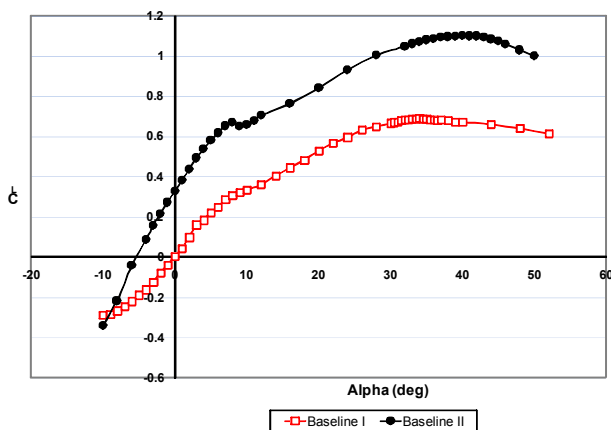


Fig 6: C_L versus α

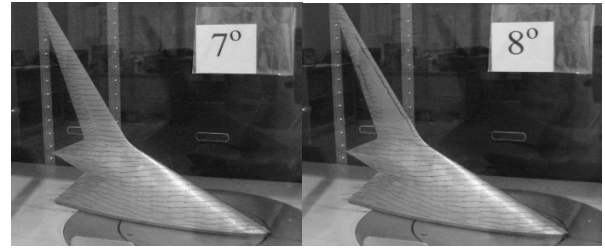


Fig 7: Visualization at $\alpha = 7^\circ$ and $\alpha = 8^\circ$

Table 2: Summary of data from C_L curves

Model	Baseline-I	Baseline-II
C_{L0}	0	0.328
$\alpha_{C_L=0}$	0	-4
C_{Lmax}	0.68	1.1
$C_{L \alpha=8}$	0.302	0.669
$C_{L \alpha=9}$	0.318	0.651

B. Drag Coefficient

Fig. 8 shows the variation of drag coefficient C_D versus angle of attack (α). The Baseline-I curve shows a constant value of C_D (around 0.03) at low angles of attack (between -10° to 8°). Deviation is observed at 8° where the wing of Baseline-I experiences stall. Beyond 8° the value of C_D then grows at higher rate as α increase. On the other hand, the Baseline-II curve also shows a constant value of C_D (around 0.03) at low angles of attack (between -10° to 8°). At 8° the curve shows a steep rise, and afterwards, C_D increases as α increases with a higher rate compared to Baseline-I. Table 3 shows some quantitative data obtained from the C_D graph.

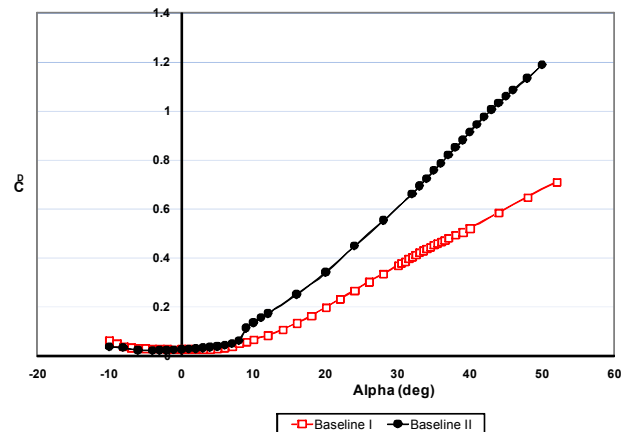


Fig 8: C_D versus α

Table 3: Summary of data from C_D curves

Model	Baseline-I	Baseline-II
C_{D0}	0.0268	0.0262
$C_{D \alpha=8}$	0.0495	0.0628
$C_{D \alpha=9}$	0.0567	0.1142

C. Lift Coefficient versus Drag Coefficient

The drag polar (C_L versus C_D) curve can be seen in Figure 9 for both models. The curve shows the value for C_D at zero lift is approximately 0.03 for both aircraft. This is the minimum drag coefficient of the BWB at zero lift (C_{D0}). It is also observed that, at high angles of attack, Baseline-II may have larger drag but at the same time it can generate higher lift.

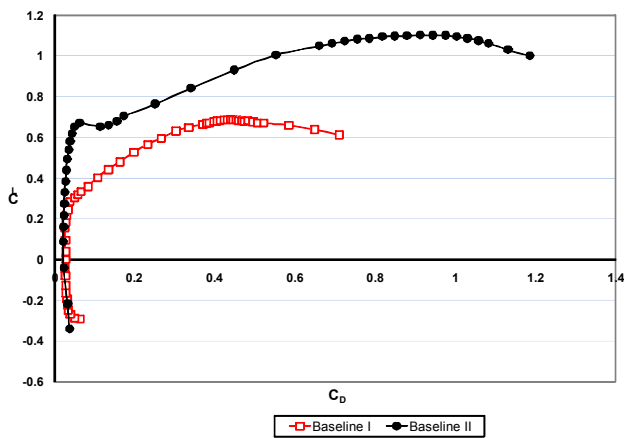


Fig 9: C_L versus C_D

D. Lift-to-Drag Ratio

Lift-to-drag ratio (L/D) versus angle of attack curves are presented in Figure 10. The Baseline-I curve shows a maximum value of L/D about 8 at $\alpha = 7^\circ$, while Baseline-II curve reaches its maximum value of about 15 at $\alpha = 5^\circ$. These angles of attack indicate the optimum flight configuration for both aircraft. This indicates that Baseline-II has better flight performance compared to Baseline-I.

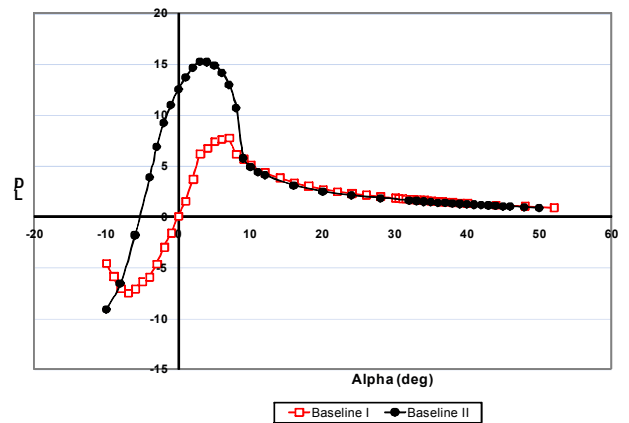


Fig 10: L/D versus α

E. Pitching Moment Coefficient

The curve of pitching moment coefficient (C_M) versus angle of attack (α) is presented in Figure 11. The measurement of pitching moment is taken at the leading edge of the models. Baseline-I has positive moment at negative angle of attack. It means that, it has a tendency to nose up during the pitching down. At positive angle of attack, pitching moments for both aircraft turn to become negative. Here also, it is noticed a small deflection of both curves around 8° which corresponds to flow separation around the wing. For Baseline-II, at $\alpha = 0^\circ$, the curve shows a slightly negative pitching moment that gives a tendency to nose down at zero degree angle of attack.

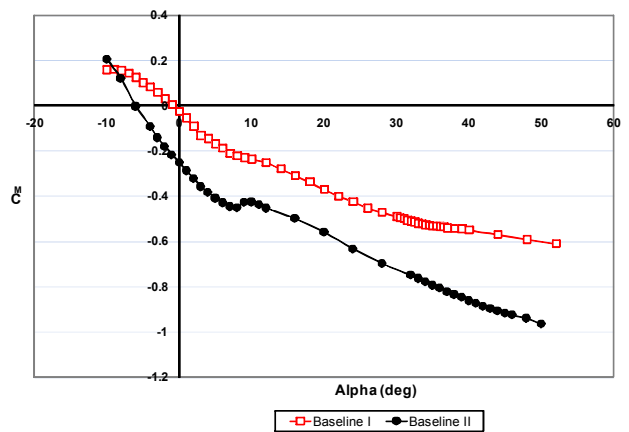


Fig 11: C_M versus α

IV. RESULTS AND DISCUSSION FOR BASELINE-I AT DIFFERENT ELEVATOR DEFLECTION ANGLE

A. Lift Coefficient

Fig.12 shows the lift coefficient versus angle of attack, α for elevator deflection from -10° to 10° . All curves have similar trends where lift coefficient increase as angle of attack increase until it reaches its maximum value at around 26° to 28° . Beyond this angle, the lift coefficient decreases. The highest lift coefficient, $C_{L,max} = 0.645$ is achieved at

angle of attack, $\alpha = 28^\circ$ for elevator deflection angle, $\alpha = 10^\circ$.

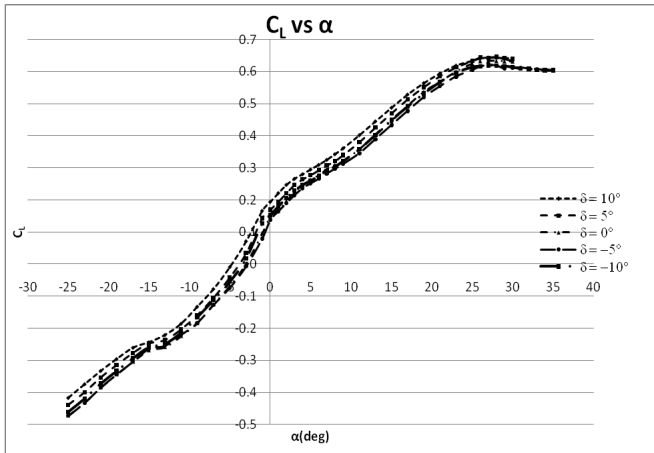


Fig 12: C_L versus α with various elevator deflection angles

Although lift curve slopes of all elevator deflection in this study is almost the same but the maximum lift at stall angle of attack of these 5 deflections are different. Downward deflections of 10° and 5° has $C_{L,max}$ of 0.645 and 0.644 respectively. Elevator deflection of 5° have stall angle, α_{stall} , of 26° , and 28° for elevator deflection of 10° . All these are higher than zero deflection with $C_{L,max}$ and α_{stall} of 0.634 and 28° respectively. Upward elevator deflections are having a lower $C_{L,max}$ and α_{stall} than zero deflection. At elevator deflection of -5° and -10° , both stall angle of attack occurred at $\alpha_{stall} = 27^\circ$ at $C_{L,max}$ of 0.620 and 0.6195 respectively.

In the low angles of attack region as shown in Fig. 13, it is observed that small elevator deflection means small lift changes. At cruising angle of attack, which occurred at $\alpha = 3^\circ$ [13], the lift increases 4% at elevator deflection angle, $\alpha = 10^\circ$ (maximum lift) compared to the elevator deflection angle, $\alpha = -5^\circ$ (minimum lift).

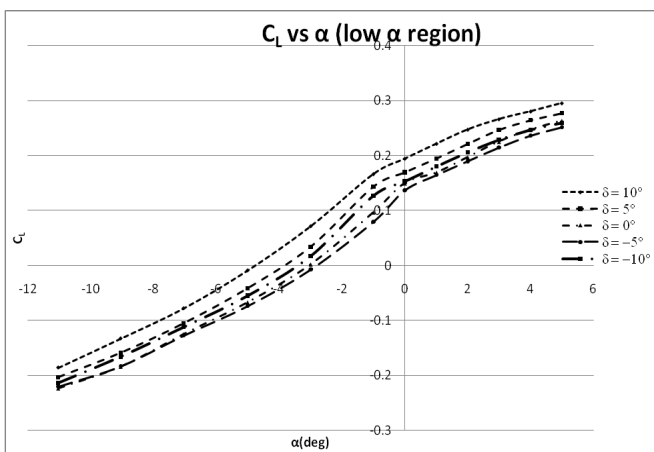


Fig 13: C_L versus α with various elevator deflection angles at low region of α

Fig. 14 show the lift coefficient versus elevator

deflection angles taken at cruising angle, 3° [13]. From the graph, it can be seen that as elevator deflection angle increase, the lift coefficient will increase. The different percentage of the lift coefficient increment/decrement with respect to the zero elevator deflection angles is show in Table 4.

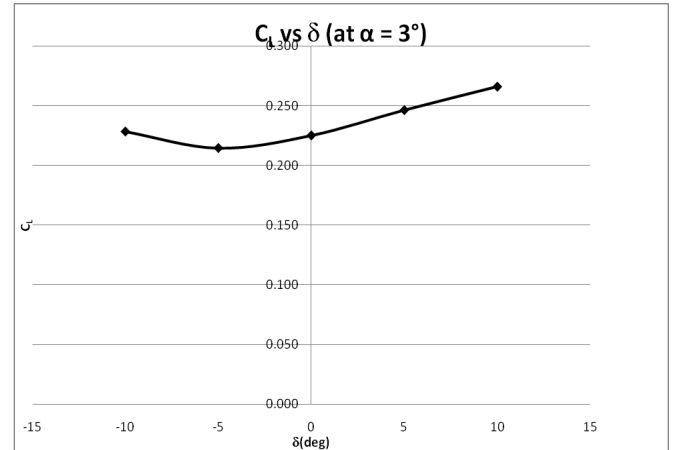


Fig 14: C_L versus elevator deflection angles

Table 4: Lift coefficient values for different elevator deflection angles

C_L	δ	%
0.228	-10	1.463
0.215	-5	-4.699
0.225	0	0.000
0.246	5	9.456
0.266	10	18.206

B. Drag Coefficient

Fig. 15 shows drag coefficient, C_D versus α . Not much change in drag is observed up to $\pm 10^\circ$ elevator deflection at low region angle of attack region but diverge at higher angle of attack region. From angle of attack -25° to -10° , the drag coefficient decrease. Then, the drag coefficient remain constant at approximately 0.03 before the drag slightly increases beyond angle of attack of 10° .

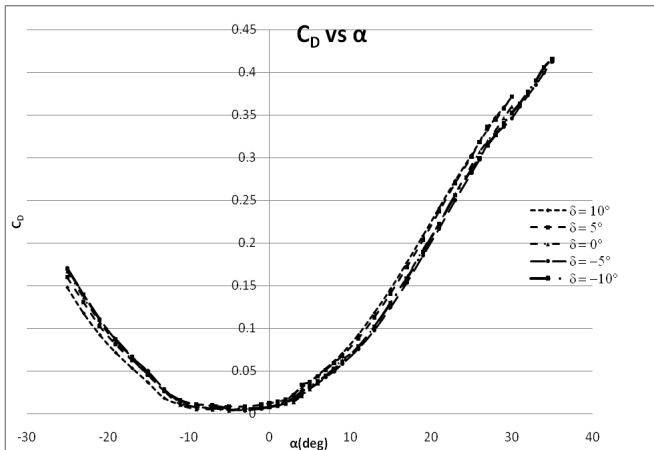


Fig 15: C_D versus α with various elevator deflection angles

In the low angles of attack region as shown in Fig. 16, it shows that at all elevator deflection greater than $\alpha = 0^\circ$, the drags increase. As elevator deflects, more resistance is observed which increase profile drag. Conventionally, the more upward or downward the deflection, the higher the drag will be.

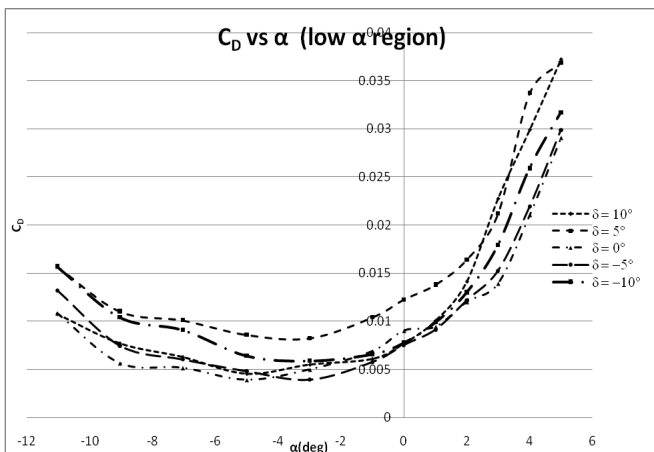


Fig 16: C_L versus α with various elevator deflection angles at low region of α

The drag coefficient versus elevator deflection angles taken at cruising angle, 3° [13] is shown in Fig. 17. Between elevator deflection angle -10° to -5° , drag coefficient is decrease and after 0° , the drag coefficient is slightly increase. The different in percentage of the drag coefficient increment/decrement with respect to the zero elevator deflection angles is show in Table 5.

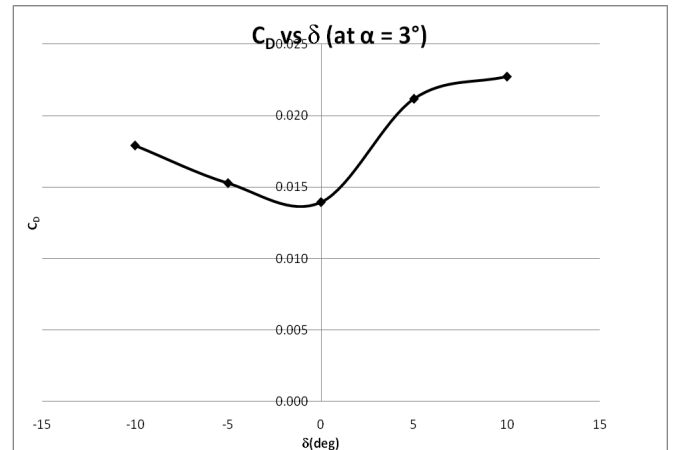


Fig 17: C_D versus elevator deflection angles

Table 5: Drag coefficient values for different elevator deflection angles

C_D	δ	%
0.018	-10	28.562
0.015	-5	9.579
0.014	0	0.000
0.021	5	52.103
0.023	10	63.274

C. Pitching Moment Coefficient

Fig. 18 shows the curves of pitching moment, C_M versus angle of attack, α . The moment coefficient is measured at the aerodynamics center AC of BWB, which is located at 36.7% reference chord, c_{ref} [13]. All the curves have the same trends, as angle of attack increases the moment will decrease. Between the angle of attack -25° to -5° , the moment coefficients have a positive value. At this point, the BWB will tend to pitch the nose upward. After this region, the moment coefficient decrease steadily and the moment coefficients are in negative value.

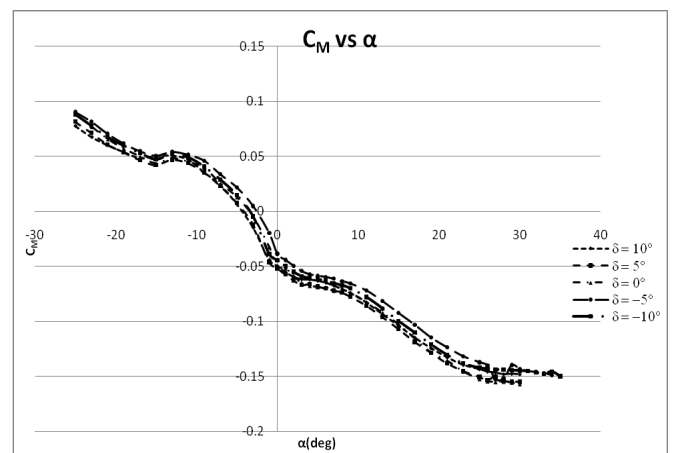


Fig 18: C_M versus α with various elevator deflection angles

Fig. 19 shows the variation of moment coefficient C_M for

different elevator deflection angles at low angles of attack.

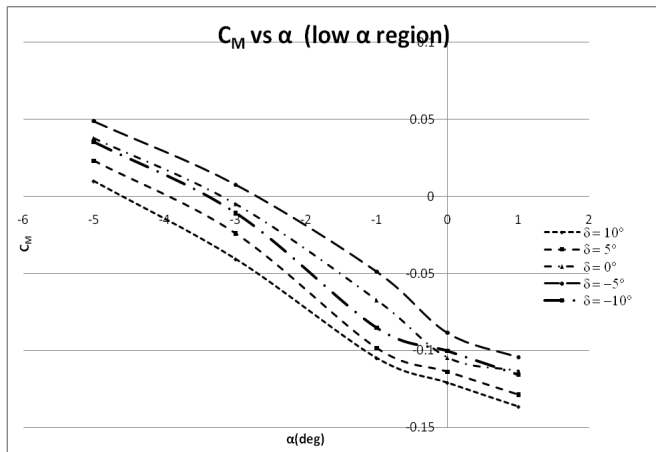


Fig 19: C_M versus α with various elevator deflection angles at low region of α

Fig. 20 show the moment coefficient versus elevator deflection angles taken at cruising angle, 3° [13]. From the graph, it can be seen that as elevator deflection angle increases, the moment coefficient will decrease, except at $\alpha = -5^\circ$. The different in percentage of the moment coefficient increment/decrement with respect to the zero elevator deflection angles is show in Table 6.

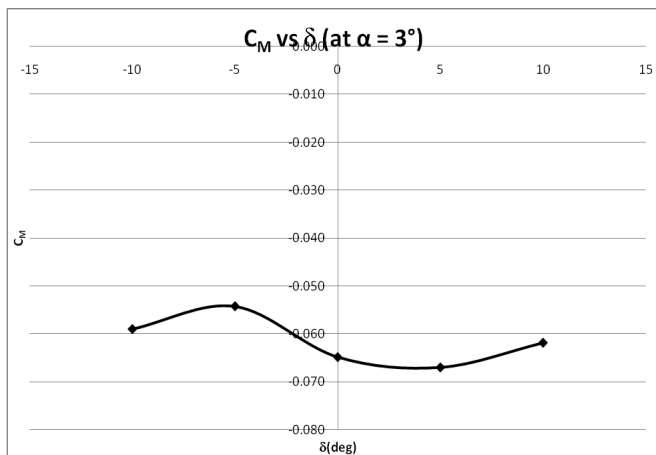


Fig 20: C_D versus elevator deflection angles

Table 6: Moment coefficient values for different elevator deflection angles

C_M	δ	%
-0.059	-10	-9.005
-0.054	-5	-16.333
-0.065	0	0.000
-0.067	5	3.316
-0.062	10	-4.611

V. RESULTS AND DISCUSSION FOR BASELINE-II AT DIFFERENT CANARD DEFLECTION ANGLE

A. Lift Coefficient

Figure 21 shows the lift coefficient versus angle of attack (α) for 6 different canard deflections. For each canard deflection, the value of C_L increases as the angle of attack increases until its maximum value around $\alpha = 40^\circ$ and decreases afterward with lower slope. Baseline II with a canard setting angle of -10 degree has a maximum lift coefficient up to 1.108. After -12° , the canard starts to contribute in producing lift (together with the wing), as it is shown by the steeper slope of the curves. The lift coefficient continues to rise until angle of attack 8° .

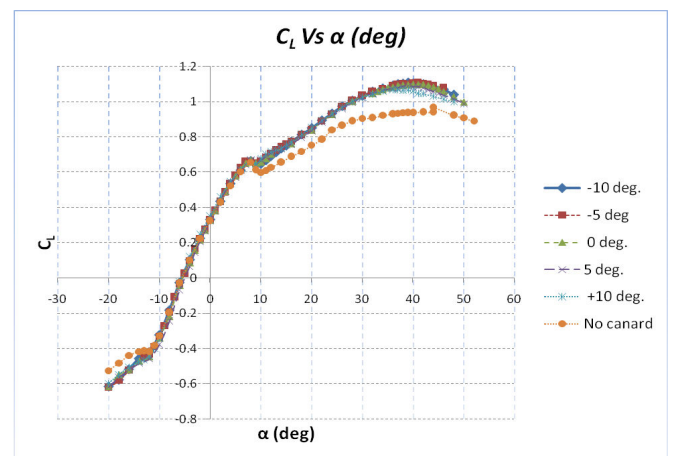


Fig 21: C_L versus α at various canard deflection angles

Zooming at the low region angle of attack as shown in Figure 22, it can be seen that at -10° , the percentage lift difference between no canard and 0° of canard deflection is 4.77%.

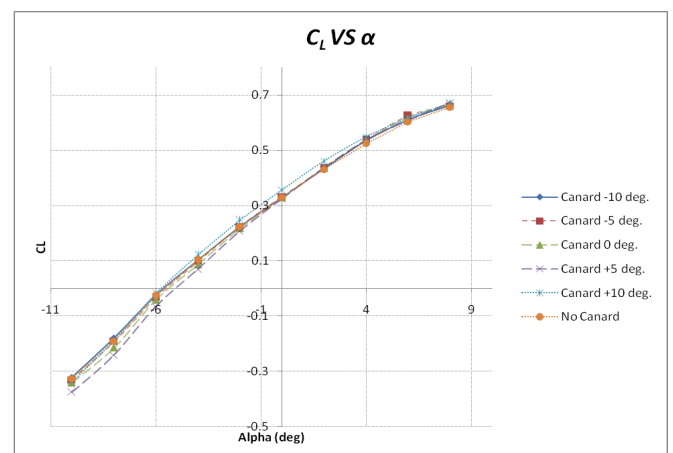


Fig 22: C_L versus α with various canard deflection angles at low region of α

From the lift coefficient at $\alpha = 0^\circ$ versus δ (deg) as shown in Figure 23, it can be observed that from -5° until

5°, the values of lift decrease but increase again at 10° and beyond. Downward deflections of canard at -5°, 0°, and 5° have C_L 0.3313, 0.3278 and 0.3249 respectively.

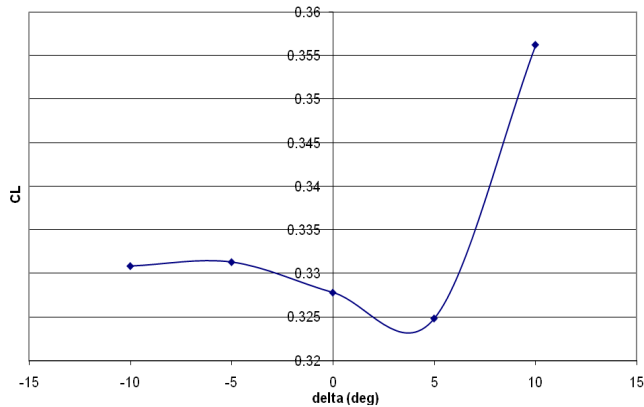


Fig 23: C_L versus canard deflection angles

B. Drag Coefficient

Figure 24 shows variation of drag coefficient (C_D) versus angle of attack (α) taken at different canard deflections with the same airspeed. Drag coefficient decreases as angle of attack increases between -20° to -8°. At 8° angle of attack, C_D increases abruptly as α is increased.

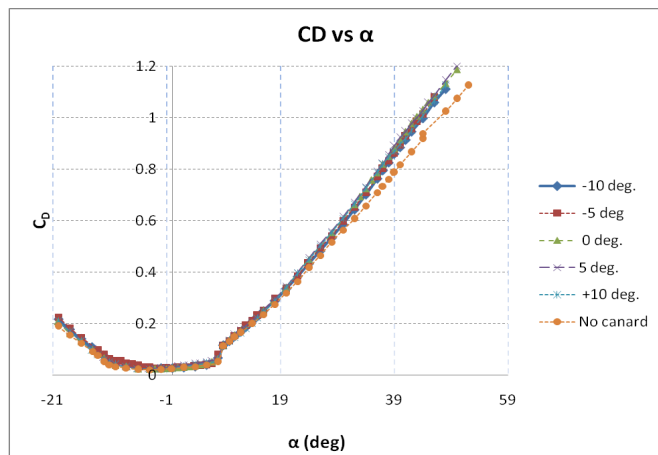


Fig 24: C_D versus α with various canard deflection angles

Figure 25 shows variation of drag coefficient (C_D) versus low region angle of attack taken at different canard deflection with same airspeed. At -10°, the difference drag between no canard and 0° of canard deflection are small. The amount is around -5.06×10^{-3} .

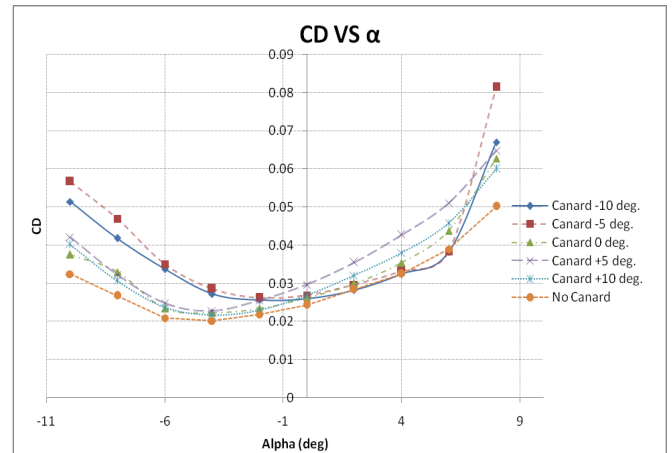


Fig 25: C_D versus α with various canard deflection angles at low region of α

Drag coefficient at $\alpha = 0^\circ$ versus δ (deg) is shown in Figure 26. At negative deflection of -10° and -5°, C_D are 0.02597 and 0.02688 respectively. While, for positive deflection of 0°, 5° and 10° the value of C_D are 0.02623, 0.02965 and 0.02685 respectively.

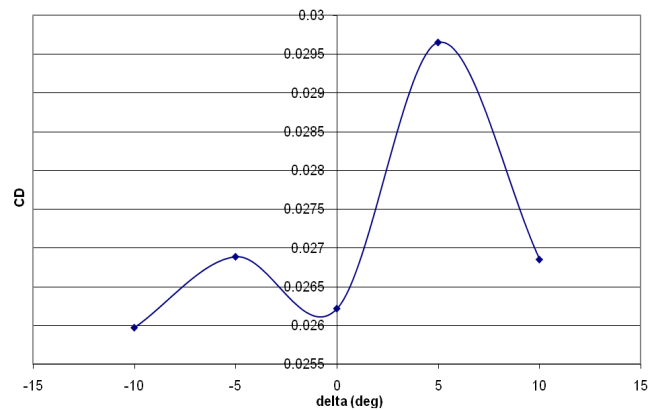


Fig 26: C_D versus canard deflection angles

C. Pitching Moment Coefficient

From the pitching moment coefficient C_M versus angle of attack α , it can be seen that, the value of C_M is fluctuating at around -20° to -12° angles of attack. The moment coefficient (C_M) is measured at aerodynamic center of the BWB. It is located at 174 mm from the leading edge.

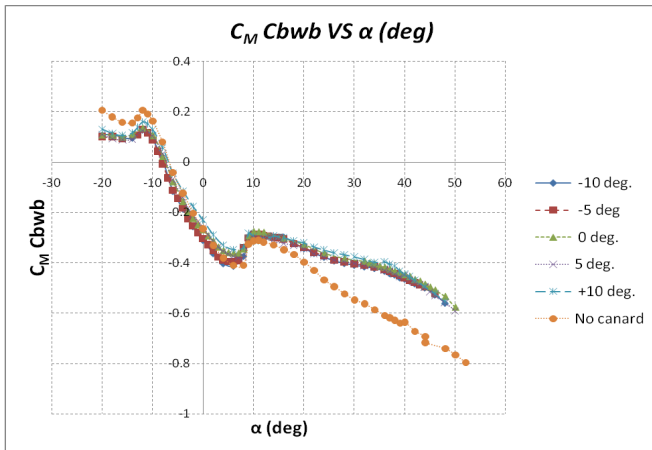


Fig 27: C_M versus α at various canard deflection angles

From the pitching moment coefficient, C_M versus angle of attack, α as shown in Figure 27, it can be seen that, the value of C_M have similar trends. As angle of attack increase, the moment will decrease. At -10° , the difference value of moment between no canard and 0° of canard deflection are small. It is around 0.0556. The curve at lower region of angle of attack is shown in Figure 28.

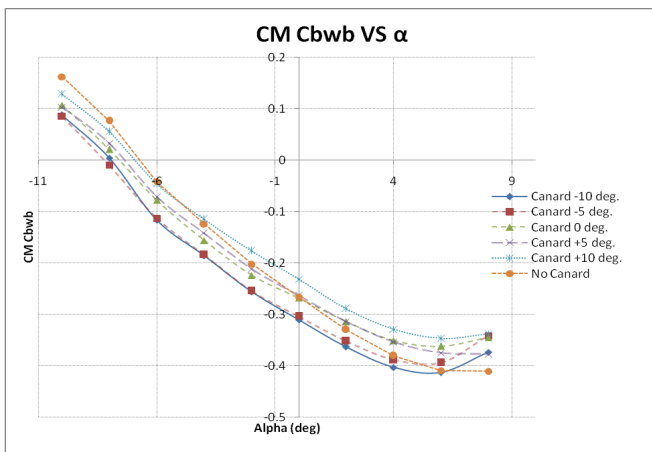


Fig 28: C_M versus α with various canard deflection angles at low region of α

The curves of pitching moment coefficient (C_M) versus canard deflection at zero angle of attack are presented in Figure 29. From the alpha at -10° until 10° , the value of moments increase with increasing canard deflection.

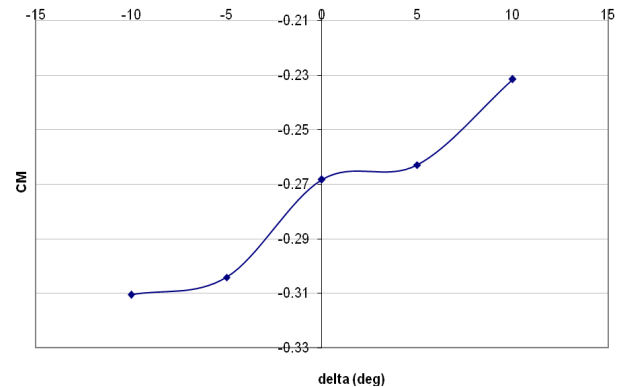


Fig 29: C_M versus canard deflection angles

VI. CONCLUSION

All data obtained from the wind tunnel experiments have been studied and analyzed to obtain aerodynamics performance characteristics of BWB Baseline-I and Baseline-II. The wind tunnel results show substantial improvement of performance for the new design Baseline-II. In terms of stall angle, Baseline-II can achieve higher stalls angle (42°) compared to its previous design (34°). The maximum Lift-to-Drag ratio obtained is approximately 15 at α around 5° for Baseline-II whereas for Baseline-I the value is approximately 8 at α around 7° . This represents better flight performance.

The experiments also were conducted with various elevator and canard deflection angles, varied from -10° to $+10^\circ$. These control surfaces are working as longitudinal motion control for both Baseline-I and Baseline-II. For zero elevator and canard deflection the results show similar trends in terms of lift curve, drag curve and pitching moment curves for both aircrafts.

As stated earlier, further investigation should be conducted to observe the phenomenon of Baseline-II that cause the lost of lift around 8° . Further study should also be carried out to minimize the disturbance effect of the canard by designing different shape of canard or reposition the canard vertically. The effect of canard deflection angles to overall performance of BWB also needs to be performed. Study on the yaw and roll direction of the BWB is also to be conducted.

REFERENCES

- [1] N. Qin, A. Vavalle, A. Le Moigne, M. Laban, K. Hackett, P. Weinerfelt. Aerodynamics Studies for Blended Wing Body Aircraft. 9th AIAA/ISSMO Symposium on Multidisciplinary Analysis and optimization, 4 – 6 September (2002), Atlanta, Georgia.
- [2] S. Siouris, N. Qin. Study of the Effects of Wing Sweep on the Aerodynamic Performance of a Blended Wing Body. (2006) Aerodynamics and Thermofluids Group, Department of Mechanical Engineering, University of Sheffield, UK.
- [3] N. Qin, A. Vavalle, A. Le Moigne, M. Laban, K. Hackett, P. Weinerfelt. Aerodynamic considerations of blended wing body aircraft. Progress in Aerospace Science (2004) pp. 321-343.
- [4] H. Engels, W. Becker, A. Morris Implementation of A Multi Level Methodology within E-Design of a Blended Wing Body. Aerospace Science and Technology (2004) pp. 145-153.

- [5] Barbara Pralio, Laura Lorefice. A Stochastic Approach to MiniUAVs Control Design. 2005 WSEAS Int. Conf. on DYNAMICAL SYSTEMS and CONTROL, Venice, Italy, November 2-4, 2005 (pp338-344)
- [6] Sepideh Afshar, Aghil Yousefi-Koma, Hossein Shahi, Donya Mohammadshahi, Hesam Maleki. Design and Fabrication of a Delta Wing Micro Aerial Vehicle. INTERNATIONAL JOURNAL OF MECHANICS Issue 4, Volume 1, 2007 pp 51-58
- [7] A. M. Mamat, R. E. Mohd Nasir, Z. Ngah, W. Kuntjoro, W. Wisnoe, R. Ramly. Aerodynamics of Blended Wing Body Unmanned Aerial Vehicle using Computational Fluid Dynamics. Journal of Mechanical Engineering, Volume 5 No. 2, October (2008) pp. 15-25.
- [8] W. Kuntjoro, R. E. Mohd Nasir, W. Wisnoe, A. M. I. Mamat, M. R. Abdullah. Computer Aided Design and Engineering of Blended Wing Body UAV. Proceedings RAeS/CEA Aircraft Structural Design Conference, 14-16 October (2008) Liverpool, UK,
- [9] W. Wisnoe, R. E. Mohd Nasir, W. Kuntjoro, A. M. I. Mamat. Wind Tunnel Experiments and CFD Analysis of Blended Wing Body (BWB) Unmanned Aerial Vehicle (UAV) at Mach 0.1 and Mach 0.3. Proceedings of the Thirteenth International Conference On Aerospace Sciences & Aviation Technology (ASAT 2009), 26-28 May (2009) Cairo, Egypt.
- [10] W. Wisnoe, W. Kuntjoro, R. E. Mohd Nasir, A. M. I. Mamat, R. Ramly. Wind Tunnel Experiments of Blended Wing Body (BWB) Unmanned Aerial Vehicle (UAV) at Loitering Phase. International Conference on Mechanical Engineering and Manufacturing. 21-23 May (2008) Johor Bahru.
- [11] R. E. Mohd Nasir, W. Kuntjoro, W. Wisnoe, A. M. I. Mamat. The Effect of Centre Elevator Deflection Aerodynamics of UiTM Baseline-I Blended Wing Body (BWB) Unmanned Aerial Vehicle) at Mach 0.3 using Computational Fluid Dynamics. Journal of Mechanical Engineering, Volume 6 No. 2, December (2009) pp. 73-96.
- [12] Rizal E. M. Nasir, Wahyu Kuntjoro, Wirachman Wisnoe, Zurriati Ali, Nor F. Reduan, Firdaus Mohamad, Shahrizal Suboh. Preliminary Design of Baseline-II Blended Wing Body (BWB) Unmanned Aerial Vehicle (UAV): Achieving Higher Aerodynamic Efficiency Through Planform Redesign and Low Fidelity Inverse Twist Method. Proceedings of EnCon2010, 3rd Engineering Conference on Advancement in Mechanical and Manufacturing for Sustainable Environment, 14-16 April (2010), Kuching, Sarawak, Malaysia,
- [13] Wirachman Wisnoe, Firdaus Mohamad, Rizal Effendy Mohd Nasir, Nor F Reduan, Zurriati Ali, Wahyu Kuntjoro, "Experimental Results Analysis of UiTM BWB Baseline-I and Baseline-II UAV Running at 0.1 Mach number", Proceedings of The 8th WSEAS International Conference on FLUID MECHANICS and AERODYNAMICS (FMA '10), Taipei, Taiwan, August 20-22, 2010
- [14] Wirachman Wisnoe, Firdaus Mohamad, Rizal Effendy Mohd Nasir, Nor F. Reduan, "Wind Tunnel Experiments Of UiTM BWB Baseline-I And Baseline-II UAV At 0.1 Mach Number", Proceedings of the 4th World Engineering Congress 2010 (WEC 2010), Kuching, Sarawak, Malaysia, August 2-5, 2010
- [15] Rizal E.M. Nasir, Wahyu Kuntjoro, Wirachman Wisnoe Zurriati M. Ali, Nor F. Reduan, Firdaus Mohamad, "The Effect of Canard on Aerodynamics and Static Stability of Baseline-II Blended Wing-Body Aircraft at Low Subsonic Speed", Proceedings of the 4th World Engineering Congress 2010 (WEC 2010), Kuching, Sarawak, Malaysia, August 2-5, 2010
- [16] Sergey A. Gaponov, Viktor Ya. Levchenko, Boris V. Smorodsky. Linear Stability of Three-Dimensional Subsonic and Supersonic Swept-Wing Boundary Layers. INTERNATIONAL JOURNAL OF MECHANICS Issue 2, Volume 2, 2008 pp 25-33
- [17] Uğur Özdemir, Elbrous M. Jafarov, Mehmet Ş. Kavsaoğlu. Calculation of the Longitudinal Stability Derivatives of a Transport Aircraft and Analysis of Longitudinal Modes. Proceedings of the 9th WSEAS International Conference on Automatic Control, Modeling & Simulation, Istanbul, Turkey, May 27-29, 2007